Acta Materialia 217 (2021) 117164

Contents lists available at ScienceDirect

Acta Materialia

journal homepage: www.elsevier.com/locate/actamat

Full length article

Measurement of Residual Stress in Silicon Carbide Fibers of Tubular Composites Using Raman Spectroscopy

James Nance[a], Ghatu Subhash[b,*], Bhavani Sankar[b], Rafael Haftka[b], Nam Ho Kim[b], Christian Deck[c], Sarah Oswald[c]

[a] University of Florida, Department of Material Science and Engineering, Gainesville, FL 32611, USA
[b] University of Florida, Department of Mechanical and Aerospace Engineering, Gainesville, FL 32611, USA
[c] General Atomics, San Diego, CA 92121, USA

ARTICLE INFO

Article history:
Received 15 February 2021
Revised 14 June 2021
Accepted 10 July 2021
Available online 15 July 2021

Keywords:
Sic fiber
Sic/sic composite
Raman spectroscopy
residual stress, graphite

ABSTRACT

Silicon carbide (SiC) fiber-reinforced ceramic matrix (SiC_f/SiC_m) composites have been identified as potential materials for nuclear fuel cladding. These composites are fabricated by braiding the SiC fibers around a mandrel into a cylindrical tube and then densifying this preform with SiC matrix using chemical vapor infiltration (CVI). However, during this fabrication process residual stresses develop in the composite, either due to the mechanical braiding process or due to high temperature CVI deposition of the SiC matrix phase. Micro-Raman spectroscopy has been employed to measure the residual stress in the SiC fibers at various stages of the fabrication process. Samples of the composite were analyzed after mechanical braiding and at 33%, 66% and 100% CVI densification of the composites. Raman spectra obtained at the above stages revealed significant band shifts of the SiC peaks and these peak-shift corresponded to -716 MPa of residual stress following the braiding process and -1075 MPa after the densification process. Interestingly, the Raman spectra also revealed carbon bands whose origin was traced to the presence of nanoscale turbostratic graphite throughout the nanograined SiC microstructure.

1. Introduction

Silicon carbide (SiC) is a structural ceramic material with applications in extreme environments including high pressure (e.g., ballistic impact [1,2]), high-temperature (e.g., turbine engines [3]) and extreme radiation (e.g., as cladding for nuclear fuel in light water reactors and in-vessel components [4,5]). It has high thermal resistance, low-thermal expansion coefficient, high oxidation resistance, and high modulus and strength [1,6]. In addition to the superior mechanical properties and chemical resistance, SiC also has a small neutron absorption cross-section and exceptional inherent radiation resistance, making it suitable for nuclear fuel cladding which experiences severe irradiation during service [7]. Recent research efforts have focused on development of accident tolerant fuel (ATF) cladding, motivated by the Fukushima-Daiichi nuclear power plant's loss-of-coolant-accident [8]. However, the major drawbacks of utilizing pure SiC in monolithic form in the aforementioned application is its low fracture toughness and brittle behavior which may cause catastrophic failure. To alleviate these concerns, continuous SiC fiber-reinforced SiC matrix (SiC_f/SiC_m) composites have been pursued [8]. Newly developed Generation-III SiC fibers used in these composites are nuclear-grade and have made SiC_f/SiC_m a viable candidate for ATF cladding. These SiC fibers with a characteristic stoichiometric ratio of Si:C exhibit properties that are much closer to that of bulk SiC compared to their predecessors [9].

To fabricate SiC_f/SiC_m composite tubes, approximately 500 SiC fibers of ~10 μm diameter are bundled together into a tow and then each tow is braided at preferred angles around a cylindrical mandrel to obtain the desired tubular fiber preform [10]. This preform is placed in a coating chamber to deposit a thin (~250-500 nm) pyrolytic carbon (PyC) interface layer around the fibers using chemical vapor deposition (CVD). Then, the tubular structure is densified with high-purity β-SiC matrix using chemical vapor infiltration (CVI) [10]. During the CVI process SiC matrix is deposited in the preform and around the SiC fibers to densify the composite structure. An X-ray computed tomography reconstruction of the SiC_f/SiC_m composite tube and a micrograph of its typical microstructure revealing the fibers and the matrix material are shown in Fig. 1. During the braiding process, the fibers are held in tension as they are braided into an overlapping woven structure, resulting in radial compression due to the overlap in the weave. This pro-

* Corresponding author.
E-mail address: subhash@ufl.edu (G. Subhash).

https://doi.org/10.1016/j.actamat.2021.117164
1359-6454/

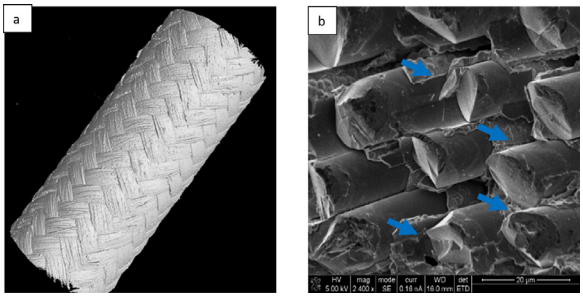

Fig. 1. (a) XCT reconstruction of a section of a woven SiC_f/SiC_m composite and (b) its microstructure revealing SiC fibers and the matrix material indicated by arrows.

cess induces complex mechanical stress state within the fibers and these stresses may remain locked-in after the composite tube is braided and densified. In addition, the high temperature deposition of β-SiC matrix onto the stoichiometric SiC fiber can induce polymorphic configurations which may result in residual thermal stresses upon cooling due to the mismatch in coefficients of thermal expansion. Therefore, it is of interest to quantitatively assess the magnitude of residual stresses in these SiC_f/SiC_m composites. However, the small fiber diameter and limited matrix material (see Fig. 1) between composites makes measuring these stresses a challenge. Residual stresses can vary dramatically over such a small region within the microstructure of the fiber. Micro-Raman spectroscopy (μRS) has been found to be an effective method to estimate local residual stresses within such small regions of a ceramic [11,12,13,14]. Raman spectroscopy is a non-destructive technique that relies on vibrational modes of bonded atoms and provides information on the phase composition, residual stress, and crystal structure of a material with a spatial resolution of approximately 1 μm. Of particular interest here is measurement of residual stress using Raman spectroscopy whose principle is based on the following: In a stress-free system, the vibrational frequencies of the crystal structure correspond to the equilibrium atomic spacing. However, when the lattice of a crystal is deformed by stress, its vibrational frequencies and hence the harmonic force constants of the lattice are altered. As a result, the Raman bands (peaks or wave numbers) are shifted in correspondence with the change in phonon frequencies of the stressed crystal. The amplitude of the shift of a specific peak (or band) in the Raman spectrum is proportional to the magnitude of the residual stress at that location [14].

In this work, we evaluated the magnitude of the residual stress developed in a SiC fiber at various stages of the fabrication process of SiC_f/SiC_m composites using Raman spectroscopy. Microstructural characterization was performed to identify the origins of the residual stresses.

2. Experimental

2.1. Composite fabrication

Generation-III Hi-Nicalon Type-S SiC fibers were chosen as the reinforcement for the SiC_f/SiC_m composites. All samples were fabricated with the same fiber batch. These fibers were synthesized by melt spinning of polycarbosilane followed by curing using electron beam irradiation and pyrolysis in a hydrogen gas flow [15]. The composite fabrication process begins with braiding SiC fiber bundles around a cylindrical mandrel to the desired $\pm 45^\circ$ reinforcement direction. After the first layer (ply) of fibers is braided on the mandrel, a second layer may be braided on top to form a 2-ply composite tube. For this study, a polymer matrix binder (Fig. 2b) was used to keep the structure of the braided fiber bundles intact to measure the residual stress before any CVI deposition. The braided tube is then placed in a CVI chamber for the deposition of a PyC interface around the individual fibers. Although in literature BN coating was used in some composites [16], for nuclear applications, boron compounds are not preferred due to their large neutron absorption cross-section and their ability to stop the nuclear reaction. A PyC interface was chosen for the composites in this study due to the retention of mechanical properties during significant radiation damage. The large porosity in the initial braided composite (see Fig. 2(a and b)) allows easy deposition around individual fibers. This interface layer between the fiber and the matrix facilitates transfer of load between the fiber and the matrix, enabling the pseudoductile behavior of SiC_f/SiC_m composites [17]. The composite is then densified with β-SiC matrix deposition through CVI, as discussed earlier. Further details of the fabrication processes are described elsewhere [10]. Select samples used in this study were removed during the CVI process at 33%, 66% and at 100% densification levels to examine the magnitude of residual stresses as a function of process time. Note that the densification with SiC matrix occurs mostly within each braid bundle in one layup as seen in images of Fig. 2 (c and e). However, when multiple lay ups exist in the composite, the inter layup space is not fully densified. Fig. 2 illustrates the structure of the composite samples at the five stages analyzed in this study.

2.2. Raman spectroscopy

Renishaw inVia Raman Microscope with a Si laser (532 nm) was used in this study. The spectrometer was coupled to a Leica optical microscope and was initially calibrated with a Si standard against the Si band position at 520 cm^{-1}. A 50 $\times$ objective lens was used to focus the incident beam on the cross section of a SiC fiber at each stage of the fabrication process (Figs. 2(c and e)) and collect the scattered beam. For comparison purposes, a bare SiC fiber was also analyzed (Fig. 2(a)), and the corresponding Raman peak positions were assumed to represent stress free measurements. All the Raman spectra were collected at room temperature. On each test sample, 10 different scans were collected from different fibers and averaged into a single spectrum for each fabrication stage. As narrated in the processing method, the SiC fibers were initially braided and then infiltrated with β-SiC using CVI. Therefore, it is hypothesized that the SiC fibers are subjected to residual stress from both the mechanical braiding and then thermal stress due to the mismatch in properties and microstructure of the stoichiometric SiC fiber and CVI infiltrated β-SiC matrix.

2.3. Transmission electron microscopy (TEM)

To understand the significance of the microstructure and its relationship with the Raman spectra, high resolution TEM investigation was performed on the bare SiC fiber. The TEM specimens were prepared from the cross section of an individual fiber using a focused ion beam (FEI Helios G4 PFIB CXe) and were observed in a field-emission TEM Talos F200i.

3. Results and discussion

3.1. Raman spectra

Fig. 3 shows Raman spectra measured on the as-received bare SiC fibers as well as on fibers after braiding into a preform, and at various stages of densification (33%, 66% and 100%). Due to the inability of being able to track an individual fiber throughout the fabrication process, spectra are taken on cross-sections of ten different SiC fibers on each specimen at the above stages and averaged. Interestingly, the observed Raman peaks in Fig. 3 not only

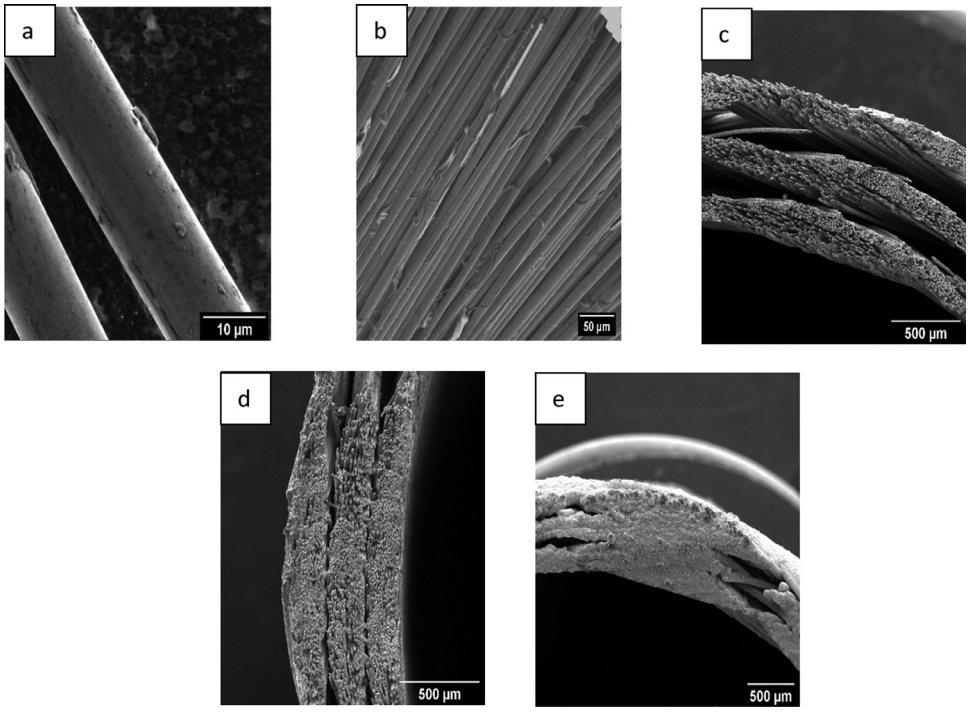

Fig. 2. Different stages of the fabrication process of SiC/SiC composites: (a) As received Hi-Nicalon Type S fibers. Micrographs along the cross-section after (b) braided fiber bundles with a polymer matrix binder as matrix before CVI, (c) after 33% of the CVI, (d) after 66% of the CVI, and (e) after 100% of the CVI.

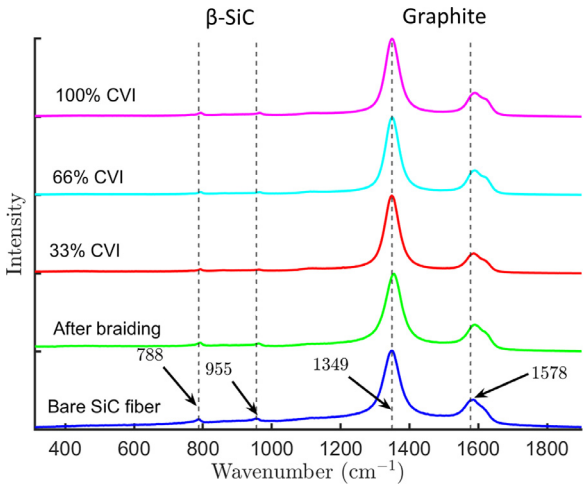

Fig. 3. Raman spectra of the SiC fiber at various stages during the CVI fabrication process.

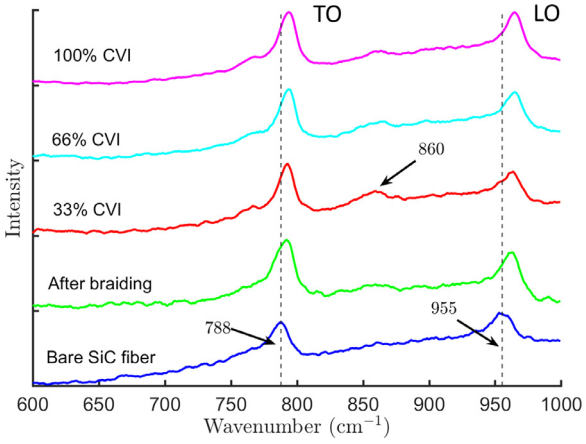

Fig. 4. Magnified view of the Raman spectra for the β-SiC section.

correspond to the vibrational modes of β-SiC but also those of graphite. The β-SiC modes are identified by the low intensity 788 cm^{-1} and the 955 cm^{-1} peaks [18], while the graphitic modes are distinguished by the high intensity 1349 cm^{-1} and the 1578 cm^{-1} peaks, traditionally called the D and the G peaks, respectively [19]. The surprising appearance of dominant graphite peaks in the Raman spectra of SiC leads us to believe that there may be residual excess carbon in the so-called stoichiometric SiC. This aspect will be explored later through transmission electron microscopy of the fiber microstructure. The over-dominance of graphite peaks compared to those of SiC is attributed to the extreme sensitivity of Raman spectroscopy to the highly symmetric covalent bonds with almost no dipole movement of graphite [20]. Also, note that the heavier Si atoms in SiC slow the vibrational frequency of the crystal and shift the corresponding Raman bands to lower frequency than those of graphite [20]. Due to the vast differences in intensities of SiC and graphite peaks, each section of the Raman spectrum is magnified and plotted separately in Figs. 4 and 5 for further analysis.

The 788 cm^{-1} peak of β-SiC corresponds to the transverse optical (TO) mode, while the 955 cm^{-1} peak corresponds to the longitudinal optical (LO) mode of the vibrations [18]. These peak positions are different from the theoretical values of 796 cm^{-1} and 971 cm^{-1} for the TO and the LO phonon peaks of β-SiC, respectively [21]. This deviation can be attributed to the observation that Hi-Nicalon Type-S SiC fibers contain a mixture of polymorphs and free carbon [9]. Therefore, in this study, the bare SiC fiber spectrum with the measured values above is taken as the stress-free state for the purposes of residual stress calculations. From Fig. 4 it is seen that the relative positions of both these peaks are shifted to the right after each fabrication stage compared to those of the

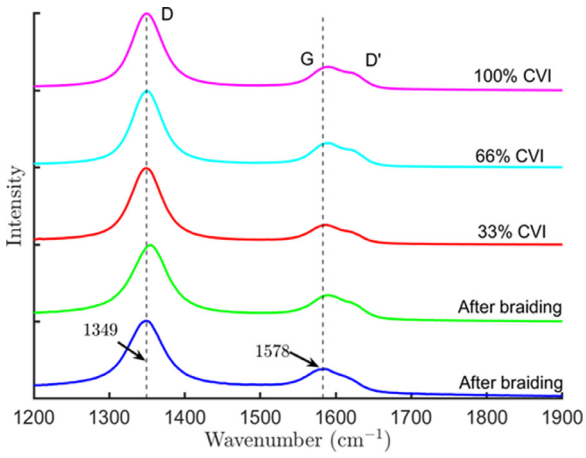

Fig. 5. Magnified view of the Raman spectra for the graphite section.

bare SiC fiber. The most significant shift in peak position for both the TO mode and the LO mode happens after the braiding process. This initial shift is 5 cm^{-1} for the TO peak and 6 cm^{-1} for the LO peak. This peak shift increases by another 2 cm^{-1} for both bands during the densification. Furthermore, a broad band, identified by an arrow in Fig. 4, begins to emerge at approximately 860 cm^{-1} during the CVI process. This could be the result of SiC polymorphs being formed during the high temperature deposition (densification) of matrix material [22].

Fig. 5 shows the magnified view of the d-peak (1349 cm^{-1}) and the G-peak (1578 cm^{-1}) of graphite. These peaks are broader (compare the base width) and not as sharp as the β-SiC peaks, reflecting the dominance of defect evolution and loss of symmetry in the crystal structure. The presence of the D and D' bands in the Raman spectrum are indicative of defect-induced Raman features in the material [23] and this band will not exist in a pure crystal with no defects. One possible explanation for the dominant D-peak is the presence of turbostratic graphite within the SiC fiber. Turbostratic graphite forms at temperatures of about 1000 °C (can exist up to 2000 °C) and consists of roughly parallel stacked layers of graphene extending over relatively small length of 1–4 nm [24]. There is no strict ordering between the adjacent layers, but can have random rotations and translations between each pair of layers. Turbostratic graphite has been shown in previous studies to be a possible explanation for a dominant D-peak in the Raman spectrum [25,26]. In the subsequent Raman analysis, the D-peak shift is not considered as it is associated with defects, and not the graphite crystal.

From Fig. 5, it is once again noted that, similar to the β-SiC peaks (Fig. 4), the most significant shift in the G peak occurs after the braiding process. This peak shift is 12 cm^{-1} and implies that the most influential processing step on the residual stresses in the SiC fibers is the mechanical braiding. There is some movement of this band beyond this processing step but it is within the statistical variability due to averaging of ten Raman scans. Furthermore, the presence of the D' peak at 1620 cm^{-1} even at the bare SiC fiber stage indicates that the turbostratic graphite is inherent to the SiC fiber [27], and this aspect will be explored next. However, during the fabrication process, the D' peak grows larger in intensity, indicating a possible influence on the SiC fibers due to the CVI process. To further confirm these features and understand the nature of the initial microstructure, high resolution transmission electron microscopy (HRTEM) was conducted of the cross-section of the SiC fibers.

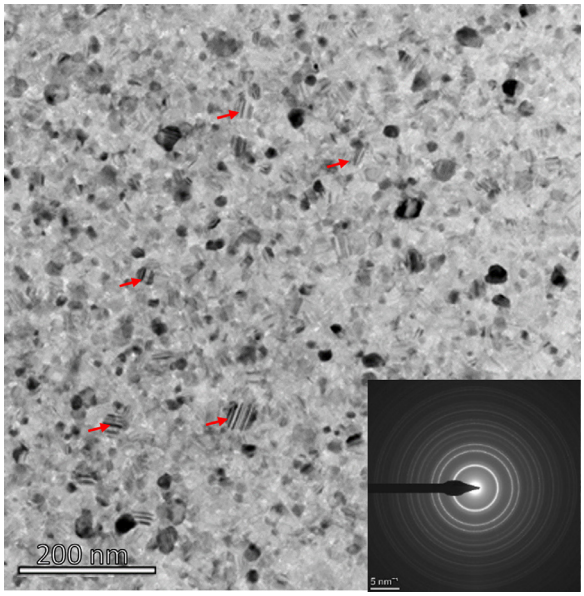

Fig. 6. TEM micrograph of the cross-section of a bare SiC fiber revealing nanoscale grains and grains with stacking faults (indicated by arrows).

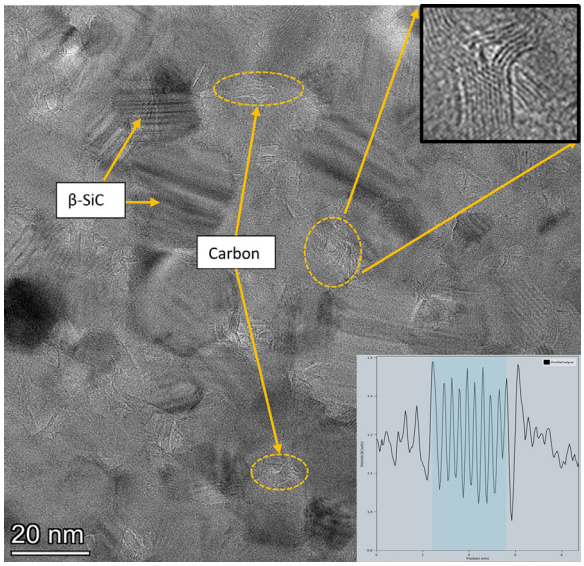

Fig. 7. High Resolution TEM micrograph revealing the presence of turbostratic graphite dispersed throughout the microstructure containing nanosized SiC grains. Spacing of the peak-intensity measurements (shown in the bottom inset) of the region (shown in the top inset) confirmed the presence of excess carbon.

3.2. HRTEM analysis

The nuclear-grade Hi-Nicalon Type-S SiC fiber is claimed to be primarily β-SiC [28]. The TEM investigations have revealed that the fiber consists of nanocrystalline β-SiC crystals of approximately 10–15 nm in size, as shown in Fig. 6. The selected area electron diffraction (SAED) pattern shows a circular ring pattern consistent with the presence of nanocrystalline grains throughout the microstructure. The β-SiC grains show high-density stacking faults, as indicated by arrows. Interestingly, the high-resolution TEM micrograph, shown in Fig. 7, reveals wavy features dispersed throughout the microstructure. These regions fit the description of turbostratic graphite (stacked parallel layers of graphene extending over 1 - 4 nm with no strict ordering, as discussed in the previous section). Signal intensity measurements, shown in the top inset of Fig. 7,

were taken across these wavy regions. The distance between the peaks of intensity is approximately 0.35 nm, which correlates well with the distance between layers of turbostratic graphite in the direction perpendicular to the c-axis in a Bernal stacking arrangement [29,30]. This observation, that there are multiple nano-scale constituents in the SiC fiber, is important. The spot size of the Raman laser is approximately one micron and the collected Raman signal averages all the nano-scale constituents. This could be a possible explanation why the as-received SiC fiber peak wavenumber is significantly different than the theoretical estimation for β-SiC (e.g., 788 cm^{-1} as opposed to 796 cm^{-1} for the TO peak) [21]. Furthermore, this observation also emphasizes the need to investigate not only the β-SiC peaks, but also the carbon peaks for residual stresses within the Hi-Nicalon Type-S SiC fibers.

3.3. Residual stress derivations and calculations

The shifts in the peak positions of the Raman spectra presented in Figs. 3-5 correspond to the residual stress induced in the material at various stages of the fabrication process. To quantify this stress, we will first derive the relationship between the stress in the material and the peak-shift from the Raman spectra through the well know phonon deformation potentials. Ganesan, et al., [31] noted that if a material is deformed due to internal or external stresses, a phenomenological approach may be adapted to describe the phonon modes. The approach consists of subjecting atoms in a crystal to generalized forces and then determining the shift in the equilibrium positions. Assuming quasi-harmonic vibrations, the new equilibrium positions of the atomic vibrations and the strain induced frequency shifts can be determined [13,32,33].

Because there are multiple constituents in the SiC fiber, separate derivations must be performed for the shifts associated with the β-SiC bonds (Fig. 4) and with the C–C bonds (Fig. 5). There are three optical phonon modes associated with β-SiC bonds - two transverse optical (TO) modes and one longitudinal optical (LO) mode [18]. The corresponding frequencies may be calculated by determining the Eigenvalues, λ_j, of the following secular equation [30]:

$$\begin{vmatrix} p\varepsilon_x^R + q\left(\varepsilon_y^R + \varepsilon_z^R\right) - \lambda_1 & r\gamma_{xy}^R & r\gamma_{xz}^R \\ r\gamma_{xy}^R & p\varepsilon_y^R + q\left(\varepsilon_x^R + \varepsilon_z^R\right) - \lambda_2 & r\gamma_{yz}^R \\ r\gamma_{xz}^R & r\gamma_{yz}^R & p\varepsilon_z^R + q\left(\varepsilon_x^R + \varepsilon_y^R\right) - \lambda_3 \end{vmatrix} = 0 \tag{1}$$

where p, q, and r are the phonon deformation potentials; ε^R and γ^R are residual normal and shear strain tensor components, respectively. For β-SiC, a zinc-blende cubic crystal structure, this relationship between stress and strain can be defined using the generalized Hooke's Law given by [32]:

$$\begin{bmatrix} \varepsilon_x \\ \varepsilon_y \\ \varepsilon_z \\ \gamma_{yz} \\ \gamma_{xz} \\ \gamma_{xy} \end{bmatrix} = \begin{bmatrix} S_{11} & S_{12} & S_{12} & 0 & 0 & 0 \\ S_{12} & S_{11} & S_{12} & 0 & 0 & 0 \\ S_{12} & S_{12} & S_{11} & 0 & 0 & 0 \\ 0 & 0 & 0 & S_{44} & 0 & 0 \\ 0 & 0 & 0 & 0 & S_{44} & 0 \\ 0 & 0 & 0 & 0 & 0 & S_{44} \end{bmatrix} \begin{bmatrix} \sigma_x \\ \sigma_y \\ \sigma_z \\ \tau_{yz} \\ \tau_{xz} \\ \tau_{xy} \end{bmatrix} \tag{2}$$

where, [S] is the compliance matrix and σ and τ represent the residual normal and shear stress components, respectively. As previously described in Section 2.1, each individual SiC fiber is surrounded by SiC matrix, and then 500 of these fibers are bundled to form a yarn. This results in a statistically sufficient number of fibers surrounding the central set of fibers in the yarn. In addition, the beam size of the Raman is only 1 μm, whereas the diameter of the fibers is approximately 10 μm. Considering both of these perspectives, it is reasonable to assume a biaxial stress state on the set of fibers that are at the center of each yarn, where the measurements for this study took place. Furthermore, because the stresses in the biaxial plane are significantly greater than the shear stresses, the shear stresses in the subsequent discussion are neglected for calculations ($\tau_{xy} = \tau_{xz} = \tau_{yz} = 0$). Lastly, it is assumed that the radial and tangential stresses are equal ($\sigma_x = \sigma_y$). Such approximations are reasonable due to the fact that the laser beam spot size on the surface is only 1 μm in diameter.

After considering the approximations, Eq. (2) reduces to:

$$\varepsilon_x^R = \left(S_{11}\sigma^R + S_{12}\sigma^R\right) \tag{3a}$$

$$\varepsilon_y^R = \left(S_{11}\sigma^R + S_{12}\sigma^R\right) \tag{3b}$$

$$\varepsilon_z^R = 2S_{12}\sigma^R \tag{3c}$$

By substituting Eqs. (3a) – (3c) into Eq. (1), the Eigenvalues can be solved as:

$$\lambda_1 = \sigma^R[p(S_{11} + S_{12}) + q(S_{11} + 3S_{12})] \tag{4a}$$

$$\lambda_2 = \sigma^R[p(S_{11} + S_{12}) + q(S_{11} + 3S_{12})] \tag{4b}$$

$$\lambda_3 = 2\,\sigma^R[pS_{12} + q(S_{11} + S_{12})] \tag{4c}$$

Assuming small deformations, the frequency associated with each mode (j = 1–3) is related to the unstrained frequency through the following relationship [18,28,31,32,33]:

$$\Delta w_j = w_j - w_{j0} \approx \frac{\lambda_j}{2w_{j0}} \tag{5}$$

We can now define the equations that relate the shift in Raman peak wavenumber, Δw_j, to the residual stresses, σ^R, as:

$$\Delta w_1 = \frac{1}{2w_1}\sigma^R[p(S_{11} + S_{12}) + q(S_{11} + 3S_{12})] \tag{6a}$$

$$\Delta w_2 = \frac{1}{2w_2}\sigma^R[p(S_{11} + S_{12}) + q(S_{11} + 3S_{12})] \tag{6b}$$

$$\Delta w_3 = \frac{1}{w_3}\sigma^R[pS_{12} + q(S_{11} + S_{12})] \tag{6c}$$

Eqs. (6a) and (6b) correspond to the TO Raman mode and Eq. (6c) corresponds to the LO Raman mode for β-SiC. For simplicity, in this study, only the TO band is used to calculate the residual stress of the β-SiC, similar to previous studies [14]. Thus, only Eqs. (6a) and (6b) will be used to calculate the residual stress from the experimental shift observed in Fig. 4. The last remaining variables to be defined are the phonon deformation potentials p and q. These values are not currently defined in literature for a zinc-blende crystal structure, however, the mode Grüneisen parameters, γ_0 and γ_S, can be used to estimate the values of p and q with fairly accurate results [18,34]. The relationship between the Grüneisen parameter and the phonon deformation potentials are given by [18]:

$$\gamma_0 = -\frac{(p + 2q)}{6w_0^2} \tag{7a}$$

$$\gamma_s = -\frac{(p - 2q)}{2w_0^2} \tag{7b}$$

The mode Grüneisen parameter for the TO phonon is defined as $\gamma_0 = 1.10$, but the value of γ_S is not readily available in β-SiC literature, therefore it is assumed that $\gamma_0 = \gamma_S = 1.10$ [35]. From Fig. 4, we measure w_0 for the bare SiC fiber in the stress-free state as 788 cm^{-1} for the TO peak and 955 cm^{-1} for the LO peak. The resulting phonon deformation potentials (from Eq. (7)) are $p = -4.554 \times 10^5$ /cm^2 and $q = -1.821 \times 10^6$ /cm^2 for the TO mode. Using these values and the defined elastic constants of β-SiC, $S_{11} = 3.7 \times 10^{-13}$

Table 1
Calculated residual stress based on TO mode for B-SiC.

Fabrication stage(cm^{-1})	Shift from stress-free state (cm^{-1})	Wavenumber	Residual Stress (MPa)
Bare SiC fiber(stress-free state)	788 ± 0.07	0	0
After braiding	792 ± 0.14	+4	−716
33% CVI	793 ± 0.14	+5	−895
66% CVI	794 ± 0.08	+6	−1075
100% CVI	794 ± 0.27	+6	−1075

Table 2
Residual stress calculations for turbostratic graphite.

Fabrication stage	Wavenumber (cm^{-1})	Shift from stress-free state (cm^{-1})	Residual Stress (MPa)
Bare SiC fiber (stress-free state)	1578 ± 0.05	0	0
After braiding	1590 ± 0.15	+12	−4.31
33% CVI	1587 ± 0.23	+9	−3.23
66% CVI	1589 ± 0.17	+11	−3.95
100% CVI	1591 ± 0.13	+13	−4.66

cm^2/dyne and $S_{12} = -1.05 \times 10^{-13}$ cm^2/dyne [36], we can now calculate the residual stress values for each shift in the Raman spectra, as summarized in Table 1 for the TO peak for β-SiC.

As indicated in Table 1, it seems that the largest influence on the residual stress (about 65% of the total stress) in the β-SiC develops during the mechanical braiding process. During the later stages of CVI densification, the peak shift is significantly smaller. The calculated residual stress is compressive in nature (indicated by the negative sign) and these stress values are in good agreement with similar work on this material. Xiao *et al.* determined the residual stresses in Hi-Nicalon Type-S SiC fibers embedded in Ti_6Al_4V matrix and found the average thermal residual stress in the fibers to be −417 MPa for the TO peak shift [33]. The difference in the magnitude of the stress between our study and that of Xiao's can be attributed to the fact that the material examined in the current study consists of a SiC matrix as opposed to a two-phase composite with Ti_6Al_4V matrix.

$$\begin{vmatrix} m(\varepsilon_x+\varepsilon_y)-\lambda & n(\varepsilon_x+\varepsilon_y) \\ n(\varepsilon_x+\varepsilon_y) & m(\varepsilon_x+\varepsilon_y)-\lambda \end{vmatrix} = 0 \tag{8}$$

For the turbostratic graphite peaks, a similar derivation is carried out but with slight differences: (i) Modifying Hooke's law for hexagonal crystal system in turbostratic graphite, as opposed to zinc blende structure of β-SiC; (ii) Only two phonon deformation potentials instead of three. In this study, we will only be defining the relationship between the Raman shift in the G-peak and the residual stress. This is done because the G-Peak is the main indicator of the presence of graphitic material in a sample and therefore gives a better representation of residual stress induced in the lattice of the turbostratic graphite. Once again, assuming $\sigma_x = \sigma_y$ in the secular Eq. (1), we redefine the equation for the G-Peak as in Eq 8, where m and n are the phonon phenomenological coefficients defined as $m = -1.44 \times 10^7 cm^{-2}$ and $n = 5.80 \times 10^6$ cm^{-2} [37,38]. Furthermore, the generalized Hooke's law for a hexagonal crystal system is now defined as:

$$\begin{bmatrix} \varepsilon_x \\ \varepsilon_x \\ \varepsilon_x \\ \gamma_{yz} \\ \gamma_{xz} \\ \gamma_{xy} \end{bmatrix} = \begin{bmatrix} S_{11} & S_{12} & S_{13} & 0 & 0 & 0 \\ S_{12} & S_{11} & S_{13} & 0 & 0 & 0 \\ S_{13} & S_{13} & S_{33} & 0 & 0 & 0 \\ 0 & 0 & 0 & S_{44} & 0 & 0 \\ 0 & 0 & 0 & 0 & S_{44} & 0 \\ 0 & 0 & 0 & 0 & 0 & 2(S_{11}-S_{12}) \end{bmatrix} \begin{bmatrix} \sigma_x \\ \sigma_y \\ \sigma_z \\ \tau_{yz} \\ \tau_{xz} \\ \tau_{xy} \end{bmatrix} \tag{9}$$

where ε_x and ε_y are residual normal strain components. Following similar methodology, as in the β-SiC case, we can define the Eigenvalues, λ_j. By substituting the stress-strain relationships into Eq. (9), and assuming small frequency deformation in Eq. 3, we can define the relationship between the Raman shift and the residual stresses as:

$$\Delta w = \frac{-\sigma}{2w_0}[(m+n)S_{11} + (m\ -\ n)S_{12}] \tag{10}$$

After substituting the defined phenomenological coefficients, elastic constants of $S_{11} = 1370 \times 10^{-6}$ MPa^{-1} and S_{12} = -148 $\times 10^{-6}$ MPa^{-1} for isotropic graphite [37], and stress-free wave numbers from Fig. 5 ($w_0 = 1578$ cm^{-1}), we can now calculate the residual stresses for each shift in Raman spectra for the G-peak, as:

$$\Delta w = 0.118\sigma \tag{11}$$

These calculated values are summarized in Table 2.

Once again, the most significant shift of the graphitic peaks occurs after the braiding of the fibers. There appears to be no significant change in the stress level after the CVI process and hence the thermal component of stress arising from the CVI processing is negligible. The turbostratic carbon experiences a compressive stress of approximately 4 MPa from mechanical braiding, while the β-SiC grains experience 716 MPa. The reason for this difference in stress level is that the graphite is surrounded by the high modulus SiC (440 GPa for SiC as opposed to 60 GPa for turbostratic graphite) which accommodates most of the mechanical stress induced by the braiding process.

We also note that both the fiber and the matrix materials being SiC (see Fig. 1), the thermal stresses are also negligible at the matrix level. Thus the compresive stress in each fiber comes from the mechanical braiding process where each tow, consisting of hundreds of fibers, is braided one over the other. However, it is difficult to assess the influence of these residual stresses on mechanical properties because both the residual stress and the structure of the composite evolve durig the fabrication process. Thus, it is difficult to fabricate a composite without these residual stresses as they are integral part of the braiding process.

Finally, we address the issue of excess carbon in the fiber microstructure. The Hi-Nicalon Type-S β-SiC fiber is promoted to be a near-stoichiometric material. However, the findings in this study reveal that there is still some turbostratic carbon dispersed at the nanoscale throughout the microstructure. Our TEM observations of excess carbon are consistent with the manufacturers data sheet which states that C/Si atomic ratio in the fiber is 1.05 [39]. Thus, there is at least 5% excess carbon in the fiber material. This study also found that the residual stress of the turbostratic graphite within the Hi-Nicalon Type-S fiber, as measured by the Raman

peak shifts, is compressive in nature. Furthermore, the presence of the turbostratic carbon in larger quantities may adversely influence the stability of the fibers and the composite in aggressive irradiation conditions [6]. Hence, manufacturers of SiC fibers should focus on further enhancement in processing conditions to eliminate the excess carbon for better radiation resistance of these composites.

4. Conclusions

Raman spectroscopic investigation of SiC_f/SiC_m composites has revealed that residual stress develops in the SiC fibers during the fabrication from two processing steps: (i) braiding of fiber bundles into a composite skeleton and (ii) high temperature densification of the composite with SiC matric using CVI. The former induces a mechanical component of residual stress while the latter induces a thermal component of residual stress upon cooling to room temperature. At the composite level, both the matrix and the fibers are made of silicon carbide and hence the residual stress from the thermal expansion mismatch will be minimal. The majority of the residual stress arises from the braiding process which induces lateral compressive stress close to 716 MPa.

Despite the claim of high purity stoichiometric composition of Hi-Nicalon Type-S SiC fibers, the Raman spectra have revealed dominant D-peak and G-peak of graphite, suggesting the presence of excess carbon in the SiC fiber. High resolution TEM analysis confirmed the presence of turbostratic graphite dispersed within the nanoscale SiC grains. These graphitic regions are subjected to stress levels in excess of 4 MPa, all of which arise from the mechanical braiding process.

Declaration of Competing Interest

The authors declare that they have no known competing financial interests or personal relationships that could have appeared to influence the work reported in this paper.

Acknowledgement

This research was performed under the Department of Energy (DOE) Nuclear Energy University Programs (NEUP) grant no. DE-NE0008773 to University of Florida.

The authors also grateful to the funding received through DoD-DURIP Instrumentation Grant “Acquisition of Upgrades for Raman Spectroscope for Enhanced Speed, UV and Polarization Capabilities” from ARO-68410-EG-RIP. The opinions expressed in this article are solely those of the authors and do not reflect those of the funding agency.

References

[1] S. Yashiro, K. Ogi, M. Oshita, High-velocity impact damage behavior of plain-woven SiC/SiC composites after thermal loading, Compos. Part B Eng. 43 (2012) 1353–1362, doi:10.1016/j.compositesb.2011.11.021.
[2] K.K. Wu, Y.L. Chen, J.N. Yeh, W.L. Chen, C.S. Lin, Ballistic impact performance of SiC ceramic-dyneema fiber composite materials, Adv. Mater. Sci. Eng. (2020) 2020, doi:10.1155/2020/9457489.
[3] G.N. Morscher, Tensile creep and rupture of 2D-woven SiC/SiC composites for high temperature applications, J. Eur. Ceram. Soc. 30 (2010) 2209–2221, doi:10.1016/j.jeurceramsoc.2010.01.030.
[4] G.M. Jacobsen, J.D. Stone, H.E. Khalifa, C.P. Deck, C.A. Back, Investigation of the C-ring test for measuring hoop tensile strength of nuclear grade ceramic composites, J. Nucl. Mater. 452 (2014) 125–132, doi:10.1016/j.jnucmat.2014.05.002.
[5] C.P. Deck, G.M. Jacobsen, J. Sheeder, O. Gutierrez, J. Zhang, J. Stone, H.E. Khalifa, C.A. Back, Characterization of SiC-SiC composites for accident tolerant fuel cladding, J. Nucl. Mater. 466 (2015) 667–681, doi:10.1016/j.jnucmat.2015.08.020.
[6] Y. Katoh, K. Ozawa, C. Shih, T. Nozawa, R.J. Shinavski, A. Hasegawa, L.L. Snead, Continuous SiC fiber, CVI SiC matrix composites for nuclear applications: properties and irradiation effects, J. Nucl. Mater. 448 (2014) 448–476, doi:10.1016/j.jnucmat.2013.06.040.
[7] G. Newsome, L.L. Snead, T. Hinoki, Y. Katoh, D. Peters, Evaluation of neutron irradiated silicon carbide and silicon carbide composites, J. Nucl. Mater. 371 (2007) 76–89, doi:10.1016/j.jnucmat.2007.05.007.
[8] K.A. Terrani, Accident tolerant fuel cladding development: promise, status, and challenges, J. Nucl. Mater. 501 (2018) 13–30, doi:10.1016/j.jnucmat.2017.12.043.
[9] A.R. Bunsell, A. Piant, A review of the development of three generations of small diameter silicon carbide fibres, J. Mater. Sci. 41 (2006) 823–839, doi:10.1007/s10853-006-6566-z.
[10] C.P. Deck, H.E. Khalifa, B. Sammuli, T. Hilsabeck, C.A. Back, Fabrication of SiC-SiC composites for fuel cladding in advanced reactor designs, Prog. Nucl. Energy. 57 (2012) 38–45, doi:10.1016/j.pnucene.2011.10.002.
[11] P. Jannotti, G. Subhash, J. Zheng, V. Halls, Measurement of microscale residual stresses in multi-phase ceramic composites using raman spectroscopy, Acta Mater 129 (2017) 482–491, doi:10.1016/j.actamat.2017.03.015.
[12] G. Parsard, G. Subhash, P. Jannotti, Amorphization-induced volume change and residual stresses in boron carbide, J. Am. Ceram. Soc. 101 (2018) 2606–2615, doi:10.1111/jace.15417.
[13] M. Shafiq, G. Subhash, A novel technique for the determination of surface biaxial stress under external confinement using raman spectroscopy, Exp. Mech. 54 (2014) 763–774, doi:10.1007/s11340-014-9851-9.
[14] A. Awasthi, G. Subhash, Deformation behavior and amorphization in icosahedral boron-rich ceramics, Prog. Mater. Sci. (2020) 112, doi:10.1016/j.pmatsci.2020.100664.
[15] Hiroshi Ichikawa, Recent advances in nicalon ceramic fibres, Ann. Chim. Sci. Mat. 25 (2000) 523–528.
[16] D. Ding, W. Zhou, F. Luo, M. Chen, D. Zhu, Dip-coating of boron nitride interphase and its effects on mechanical properties of SiC f/SiC composites, Mater. Sci. Eng. A. 543 (2012) 1–5, doi:10.1016/j.msea.2012.01.118.
[17] B. Yang, X. Zhou, Y. Chai, Mechanical properties of SiCf/SiC composites with PyC and the BN interface, Ceram. Int. 41 (2015) 7185–7190, doi:10.1016/j.ceramint.2015.02.041.
[18] F. Cerdeira, C.J. Buchenauer, F.H. Pollak, M. Cardona, Stress-induced shifts of first-order raman frequencies of diamond- and zinc-blende-type semiconductors, Phys. Rev. B. 5 (1972) 580–593, doi:10.1103/PhysRevB.5.580.
[19] E. López-Honorato, P.J. Meadows, R.A. Shatwell, P. Xiao, Characterization of the anisotropy of pyrolytic carbon by raman spectroscopy, Carbon N. Y. 48 (2010) 881–890, doi:10.1016/j.carbon.2009.11.010.
[20] J. Hodkiewicz, Characterizing carbon materials with raman spectroscopy, (2010). 10.1021/jp0215217.
[21] H. Okumura, E. Sakuma, J.H. Lee, H. Mukaida, S. Misawa, K. Endo, S. Yoshida, Raman scattering of SiC: application to the identification of heteroepitaxy of SiC polytypes, J. Appl. Phys. 61 (1987) 1134–1136, doi:10.1063/1.338157.
[22] D. Frazer, M.D. Abad, D. Krumwiede, C.A. Back, H.E. Khalifa, C.P. Deck, P. Hosemann, Localized mechanical property assessment of SiC/SiC composite materials, Compos. Part A Appl. Sci. Manuf. 70 (2015) 93–101, doi:10.1016/j.compositesa.2014.11.008.
[23] L.M. Malard, M.A. Pimenta, G. Dresselhaus, M.S. Dresselhaus, Raman spectroscopy in graphene, Phys. Rep. 473 (2009) 51–87, doi:10.1016/j.physrep.2009.02.003.
[24] T. Zheng, J.N. Reimers, J.R. Dahn, Effect of turbostratic disorder in graphitic carbon hosts on the intercalation of lithium, Phys. Rev. B. 51 (1995) 734–741, doi:10.1103/PhysRevB.51.734.
[25] A.C. Ferrari, J.C. Meyer, V. Scardaci, C. Casiraghi, M. Lazzeri, F. Mauri, S. Piscanec, D. Jiang, K.S. Novoselov, S. Roth, A.K. Geim, Raman spectrum of graphene and graphene layers, Phys. Rev. Lett. 97 (2006) 1–4, doi:10.1103/PhysRevLett.97.187401.
[26] P. Ruz, S. Banerjee, M. Pandey, V. Sudarsan, P.U. Sastry, R.J. Kshirsagar, Structural evolution of turbostratic carbon: implications in H2 storage, Solid State Sci 62 (2016) 105–111, doi:10.1016/j.solidstatesciences.2016.10.017.
[27] N. Ferralis, Probing mechanical properties of graphene with raman spectroscopy, J. Mater. Sci. 45 (2010) 5135–5149, doi:10.1007/s10853-010-4673-3.
[28] M. Takeda, A. Urano, J.I. Sakamoto, Y. Imai, Microstructure and oxidative degradation behavior of silicon carbide fiber hi-nicalon type S, J. Nucl. Mater. 258–263 (1998) 1594–1599, doi:10.1016/S0022-3115(98)00223-2.
[29] D.D.L. Chung, Review: graphite, J. Mater. Sci. 37 (2002) 1475–1489, doi:10.1023/A:1014915307738.
[30] L.M. Malard, M.A. Pimenta, G. Dresselhaus, M.S. Dresselhaus, Raman spectroscopy in graphene, Phys. Rep. 473 (2009) 51–87, doi:10.1016/j.physrep.2009.02.003.
[31] S. Ganesan, U. States, A. Force, A.C. Scientific, A lattice theory of morphic effects in crystals of the diamond structure, Physics (College. Park. Md). 594 (1970) 556–594.
[32] D. Ghosh, G. Subhash, N. Orlovskaya, Measurement of scratch-induced residual stress within SiC grains in ZrB2-SiC composite using micro-raman spectroscopy, Acta Mater 56 (2008) 5345–5354, doi:10.1016/j.actamat.2008.07.031.
[33] Z. Xiao, Y. Yang, N. Jin, S. Liu, X. Luo, B. Huang, Microstructure and thermal residual stress analysis of SiC fiber through raman spectroscopy, J. Raman Spectrosc. 44 (2013) 1306–1311, doi:10.1002/jrs.4356.
[34] Z.C. Feng, W.J. Choyke, J.A. Powell, Raman determination of layer stresses and strains for heterostructures and its application to the cubic SiC/Si system, J. Appl. Phys. 64 (1988) 6827–6835, doi:10.1063/1.341997.
[35] A. Debernardi, C. Ulrich, K. Syassen, M. Cardona, Raman linewidths of optical phonons in 3c-sic under pressure: first-principles calculations and experimental results, Phys. Rev. B - Condens. Matter Mater. Phys. 59 (1999) 6774–6783, doi:10.1103/PhysRevB.59.6774.

[36] M. Miura, H. Murata, Y. Shiro, K. Iishi, Ionicity scale and piezoelectricity of crystals with zincblende- and wurtzite-type structure, J. Phys. Chem. Solids. 42 (1981) 931–936, doi:10.1016/0022-3697(81)90020-2.
[37] R. Krishna, A.N. Jones, R. Edge, B.J. Marsden, Residual stress measurements in polycrystalline graphite with micro-raman spectroscopy, Radiat. Phys. Chem. 111 (2015) 14–23, doi:10.1016/j.radphyschem.2015.02.007.
[38] H. Sakata, G. Dresselhaus, M.S. Dresselhaus, M. Endo, Effect of uniaxial stress on the raman spectra of graphite fibers, J. Appl. Phys. 63 (1988) 2769–2772, doi:10.1063/1.340975.
[39] T. Ishikawa, Advances in inorganic fibers, Adv. Polym. Sci. 178 (2005) 109–144, doi:10.1007/b104208.